Journal of Solid State Chemistry 181 (2008) 2133–2138

Contents lists available at ScienceDirect

Journal of Solid State Chemistry

journal homepage: www.elsevier.com/locate/jssc

Wet chemical synthesis and photocatalytic activity of potassium niobate $K_6Nb_{10.8}O_{30}$ powders

Gaoke Zhang *, Yanjun Hu, Xinmiao Ding, Jin Zhou, Junwei Xie

School of Resources and Environmental Engineering, Wuhan University of Technology, Luoshi Road 122, Wuhan 430070, PR China

ARTICLE INFO

Article history:
Received 14 August 2007
Received in revised form
29 January 2008
Accepted 29 April 2008
Available online 8 May 2008

Keywords:
$K_6Nb_{10.8}O_{30}$
Niobate
Tungsten bronze structure
Wet chemical synthesis
Photocatalytic activity
Acid red G

ABSTRACT

The nanometer potassium niobate powders with tungsten bronze (TB)-type structure were synthesized by a wet chemical method and characterized by X-ray diffraction (XRD) and field emission scanning electron microscope (FESEM). X-ray photoelectron spectroscopy (XPS) analysis confirmed the niobium with mixed valence states exists in the crystal structure of the photocatalyst, which may be advantage for increasing the photocatalytic activity. The band gap of $K_6Nb_{10.8}O_{30}$ powders was estimated to be about 2.92 eV and shows a markedly blue-shift as compared to that of the sample obtained by the solid-state reaction. The photocatalytic activity of the samples was evaluated by degradation of acid red G under UV irradiation and the photocatalytic reaction follows first-order kinetics. The photocatalytic activity of the as-prepared sample is much higher than that of sample synthesized by solid-state reaction, and slightly higher than that of P25-TiO_2.

1. Introduction

A large quantity of highly colored wastewater from the textile industry is toxic and mostly nonbiodegradable and also resistant to destruction by conventional physico-chemical treatment methods, such as chemical precipitation and separation of pollutants, electrocoagulation [1], adsorption by activated carbon [2], coagulation [3], etc., which cannot eliminate the contamination completely but only transfer it from one phase to another. Heterogeneous photocatalysis has been considered as a cost-effective alternative for the purpose of efficiently purifying the dye-containing wastewater [4–6].

Although titanium dioxide is the most widely used photocatalyst, which is capable of decomposing a wide variety of organic and inorganic pollutants and toxic materials [7–9], their reactivity and selectivity are still not enough for large-scale applications. Many attentions have been paid for finding more efficient photocatalysts. Some layered niobate compounds, such as $K_4Nb_6O_{17}$ [10], KNb_3O_8 [11,12], NiM_2O_6 (M = Nb, Ta) [13], $BiNbO_4$ [14], NiO-$KTiNbO_5$ [15], etc., have attracted special attention because of their excellent photocatalytic activity in the field of water splitting to H_2 and O_2 or the photocatalytic degradation of organic pollutants.

Most of niobates were usually synthesized by solid-state reaction and with larger crystal size, which may decrease their catalytic activity. Some modified solid-state reaction and wet chemical methods were studied to prepare the niobate powders. Liu and Xue [16,17] obtained high-quality lithium niobate powders by modified solid-state reaction using niobium oxide and activated niobium oxide as Nb sources, respectively. Lithium niobate oxide also was prepared by wet chemical method or soft chemical method [18–23]. We first reported the photocatalytic activity of niobate $K_6Nb_{10.8}O_{30}$ with tungsten bronze (TB)-type structure, which was obtained by solid-state reaction method [24]. The crystal structure of $K_6Nb_{10.8}O_{30}$ is constructed by NbO_6 octahedra, which form some triangle, quadrilateral and pentagonal tunnels. The pentagonal and quadrilateral tunnels are occupied by K cations and the triangle tunnels are occupied by Nb cations [25,26]. In this paper, the nanometer niobate $K_6Nb_{10.8}O_{30}$ with TB-type potassium was prepared by wet chemical synthesis using niobium oxide and potassium nitrate as raw materials at low temperature and shows very high photocatalytic activity for the degradation of acid red G under UV irradiation.

2. Experimental

2.1. Synthesis of the photocatalysts

Potassium nitrate (KNO_3), niobium pentoxide (Nb_2O_5), oxalic acid (OA), citric acid (CA), ethylene glycol (EG) and hydrochloric acid (HCl) were used as starting materials. Citric acid and ethylene glycol were used as the chelating agent and esterification agent, respectively. All chemicals used in the experiment were analytical

* Corresponding author. Fax: +86 27 87887445.
E-mail address: gkzhang@whut.edu.cn (G. Zhang).

0022-4596/$ - see front matter © 2008 Elsevier Inc. All rights reserved.
doi:10.1016/j.jssc.2008.04.035

reagent grade without further purification. Deionized water was used in the whole experiment.

The flowchart for the synthesis of $K_6Nb_{10.8}O_{30}$ powders is shown in Fig. 1. About 1–2 g of Nb_2O_5 powder was added to 70 ml of 2–3 mol/L KOH solution, which was loaded into a 100 cm^3 Teflon-lined cylindrical autoclave. Then the sealed autoclave was heated at 200 °C for 4 h, a clear solution was obtained. The pH of the solution was slowly and accurately adjusted to 5.5 by dropwise adding HCl solution and the precipitated niobic acid was filtered and washed to eliminate all potassium ions [12,21]. Freshly precipitated niobic acid was added into an aqueous solution of oxalic acid. The solution was stirred at 80 °C until all niobic acid was dissolved. The concentration of niobium in the solution was determined by ICP spectrometry. For the preparation of the K–Nb precursor solution, Nb–OA complex and KNO_3 were mixed together with the molar ratio 6:10.8 of K:Nb, followed by the addition of citric acid in the molar ratio 3:1 of CA/metal cations. After homogenization, ethylene glycol was added to this solution to promote polymerization of the mixed citrate and the mass ratio of CA/EG was 60/40. The solution was stirred at 80 °C for 2 h so as to promote the solubility. Furthermore, the aqueous solvent was slowly evaporated until the formation of dark-colored, amorphous citrate gels and polymeric precursors, which were kept at 450 °C for 4 h to remove the organics, then calcined at various temperatures for different times.

The pure $K_6Nb_{10.8}O_{30}$ powders were also prepared by the solid-state reaction at 1000 °C for 2 h using niobium oxide and potassium carbonate (K_2CO_3) as raw materials.

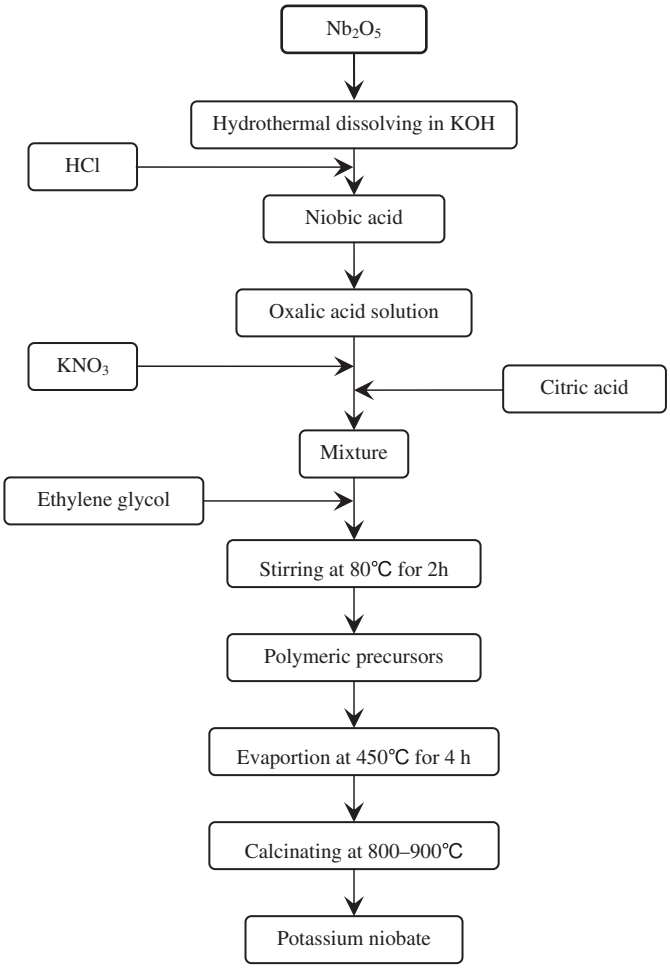

Fig. 1. Flowchart for the synthesis of $K_6Nb_{10.8}O_{30}$.

2.2. Photocatalytic experiments

The photodegradation of acid red G aqueous solution was carried out in a 500 ml Pyrex glass vessel with constant magnetic stirring at room temperature. A 20 W UV lamp ($\lambda = 253.7$ nm) was used as light source with light intensity 0.524 mW/cm^2 measured by UV-B radiatometer. Reaction suspension was prepared by adding 150 mg of the as-prepared sample into 150 ml acid red G aqueous solution (50 mg/L). The distance between the liquid surface and the light source was about 8 cm. The suspensions were first stirred in the dark for 10 min to reach equilibrium sorption of the dye. Analytical samples were drawn from the reaction suspensions after various reaction times and centrifuged at 2000 rpm for 40 min to separate the particles. The concentrations of acid red G were analyzed by UV–Vis spectroscopy (UV-751GD) at its maximum absorption wavelength of 505 nm. The linear relationship between the absorbance at 505 nm (A) and the concentration of acid red G (C) (mg/L) can be represented empirically by the equation [24]

$$A \approx 0.01C \quad \text{(a)}$$

The photodegradation rate (X) was given by $X = (C_0 - C)/C_0 \approx (A_0 - A)/A_0$, where C_0 is initial concentration of acid red G.

The photocatalytic properties of the sample obtained by solid-state reaction and P25-TiO_2 powder were determined and compared with the as-prepared sample.

3. Results and discussion

3.1. XRD patterns analysis

The phase composition and crystallinity of the synthesized powders were analyzed using powder X-ray diffraction (XRD) method, which were carried out on D/MAX-RB powder X-ray diffractometer (Rigaku, Japan) in the 2θ range from 5° to 70°. Fig. 2(a) shows the XRD pattern of the as-prepared $K_6Nb_{10.8}O_{30}$ powder at 800 °C for 24 h, which can be identified and indexed using the standard XRD data of $K_6Nb_{10.8}O_{30}$ (JCPDS 87-1856). XRD peaks of $K_6Nb_{10.8}O_{30}$ can nearly match up to the standard XRD peaks and are with the large width of the peaks, which show the prepared sample consists of a nearly single phase of the compound $K_6Nb_{10.8}O_{30}$ and its crystal particle size is small. As a

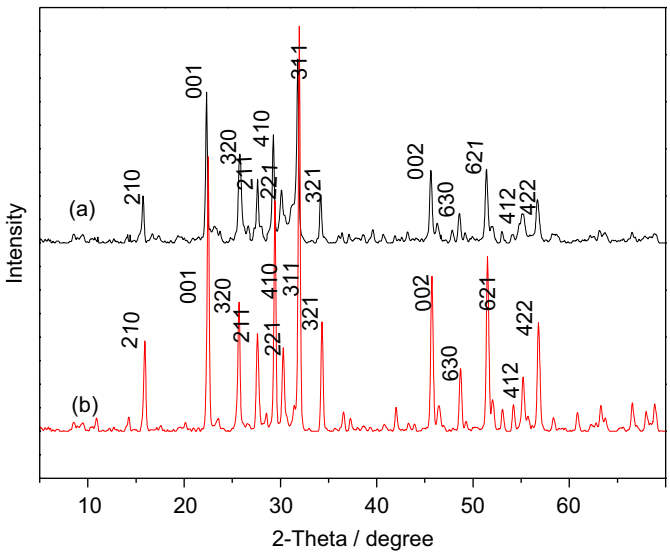

Fig. 2. Powder XRD patterns of $K_6Nb_{10.8}O_{30}$ (a) prepared by the wet chemical method calcined at 800 °C and (b) obtained by the solid-state method.

comparison, the XRD pattern of the powder prepared by the solid-state reaction method shows the sharp peaks and the small width of the peaks (Fig. 2(b)), which indicates the crystal particle size of the sample is larger.

3.2. SEM analysis

The crystal morphologies of as-prepared powder prepared by the wet chemical method were investigated using a S-4800 field emission scanning electron microscope (FESEM) and the sample obtained by solid-state reaction was observed with JSM-5610LV scanning electron microscopy (SEM). A typical low-magnification FESEM image of $K_6Nb_{10.8}O_{30}$ powders prepared by the wet chemical method is shown in Fig. 3(a). It can be seen that the particles show high dispersivity and uniform shape and size. As shown from a higher-magnification FESEM image in Fig. 3(b), $K_6Nb_{10.8}O_{30}$ particles show tetragonal columnar shape and are with an average diameter 50–150 nm and the length of 250–400 nm. Fig. 3(c) shows the low-magnification SEM image of $K_6Nb_{10.8}O_{30}$ powders prepared by solid-state reaction, which indicates the $K_6Nb_{10.8}O_{30}$ powders consist of the big aggregates of particles. A closer examination of the samples indicates that the particle size is about 1.5–3.0 μm and much bigger than that of the samples by wet chemical method. The results may be attributed to these reasons: (a) the niobic acid in wet chemical method is more reactive than niobium oxide in the solid-state reaction [21]; (b) the Nb–OA complex and KNO_3 in the K–Nb precursor solution can be mixed completely and their reactive activity is higher than that of Nb_2O_5 and K_2CO_3 in the solid-state reaction system, which improves homogeneity.

3.3. XPS analysis

X-ray photoelectron spectroscopy (XPS) analysis is an important method for the analysis of the Nb chemical state of niobates [27–30]. Tabata et al. [31] reported the XPS study of $LiNbO_3$, the results showed Nb in the obtained sample exists in Nb^{5+} and Nb^{4+}. The high-resolution XPS spectra of the Nb3d region of the as-prepared catalyst are shown in Fig. 4. The Nb3d region is composed of Nb3d5/2 peak and Nb3d3/2 peak, which can be fitted into six peaks. Generally, the Nb3d5/2 binding energy of the Nb^{4+} in niobate is about 205.5 eV, and the Nb3d5/2 binding energy of the Nb^{5+} in niobate is 206.5–207.2 eV [31–34]. The binding energy of the Nb^{5+} is higher than that of the Nb^{4+}. The two main peaks in Fig. 4 are the Nb3d5/2 peak and Nb3d3/2 peak in Nb^{5+} (1) O_6 octahedra at binding energies of 206.7 and 209.31 eV. The higher binding energy peaks belong to the Nb3d5/2 peak and Nb3d3/2 peak of the Nb^{5+} (2) in Nb (2) O_6 octahedra at binding

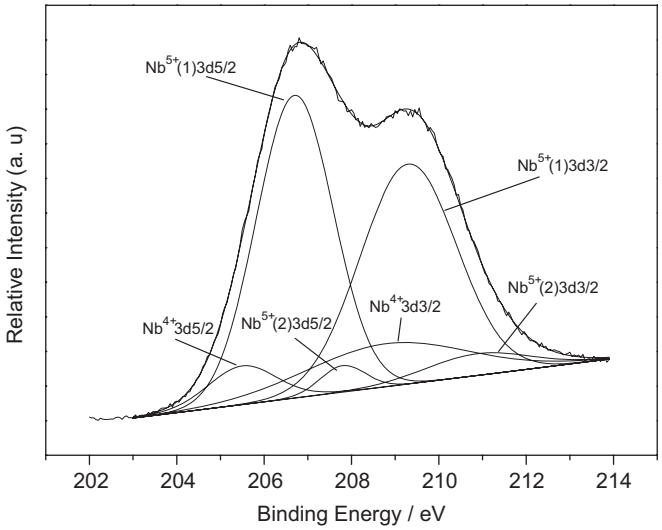

Fig. 4. High-resolution XPS spectra of the Nb3d region of the catalyst.

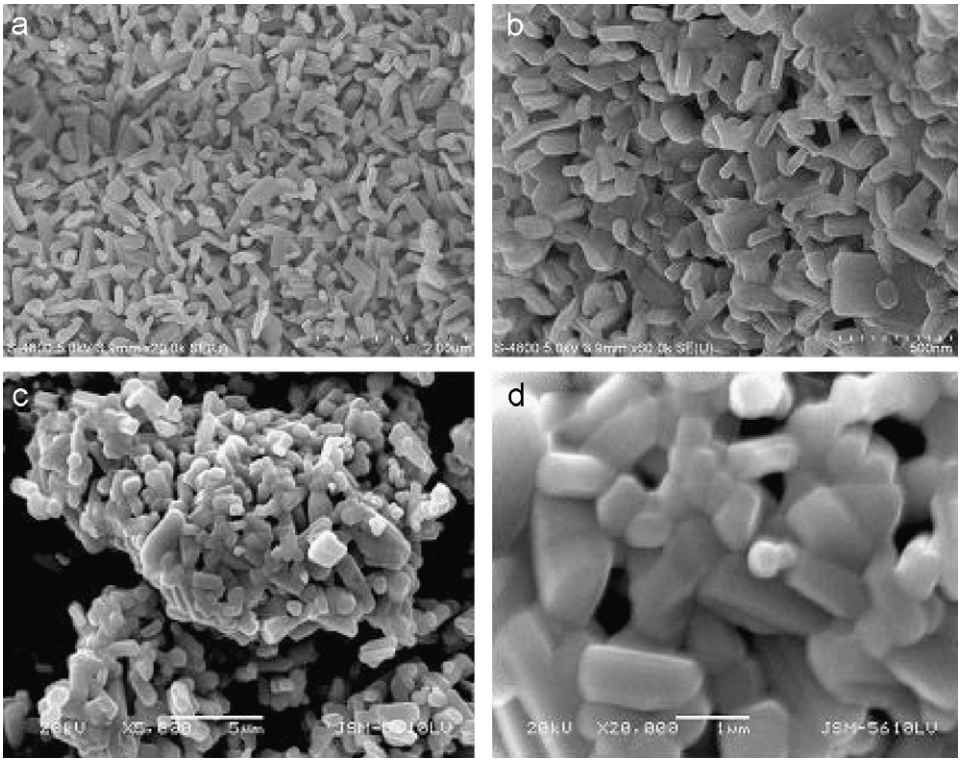

Fig. 3. SEM images of the as-prepared $K_6Nb_{10.8}O_{30}$ powders by the wet chemical method calcined at 800 °C ((a) low magnification view image and (b) high magnification view image) and by the solid-state reaction ((c) low magnification view image and (d) high magnification view image).

energies of 207.8 and 210.88 eV. The lower binding energy peaks (205.6, 208.56 eV) are attributed to the Nb3d5/2 peak and the Nb3d3/2 peak of the Nb^{4+} (3) [34,35]. The results of curve fitting of XPS spectra of the Nb3d region of the catalyst are listed in Table 1, where r_i (%) is the ratio of each kind contribution to the total of all the three kinds of niobium contributions. By XPS analysis, Cabrera et al. [36] reported that dioxide carbon can affect the Nb chemical state of lithium niobate. The results in Fig. 4 and Table 1 reveal that Nb^{4+} exists in the structure of the compound $K_6Nb_{10.8}O_{30}$ and the amount of Nb^{4+} in the crystals is more than that of the sample obtained by the solid-state reaction method [24,34,35], which may be attributed to the reduction effect of carbon in wet chemical process and XPS survey spectrum (Fig. 5) indicates that there is C element in the sample.

3.4. UV–Vis diffuse reflectance spectrum

UV–Vis diffuse reflectance analysis of $K_6Nb_{10.8}O_{30}$ was performed on UV–Vis spectrometer (UV2550, Shimadzu, Japan; $BaSO_4$ was used as a reference). As shown in Fig. 6, the absorption edge (Fig. 6(a)) of the catalyst $K_6Nb_{10.8}O_{30}$ obtained by wet chemical method is estimated to be 424.45 nm, corresponding to the band gap energy of 2.92 eV, which shows a markedly blue-shift as compared to that of the sample obtained by the solid-state reaction (Fig. 6(b)). The result may be ascribed to the quantum size effect of the $K_6Nb_{10.8}O_{30}$ particles obtained by wet chemical method, which is consistent with the results of XRD and FESEM analyses.

3.5. Photocatalytic activity of photocatalysts

The photocatalytic property of the catalyst was evaluated by the degradation of acid red G over the photocatalyst under UV

Table 1
Results of curve-fitting of the high-resolution XPS spectra of the Nb3d region

	Nb^{5+} (1)	Nb^{5+} (2)	Nb^{4+} (3)
Nb3d5/2 E_b (eV)	206.70	207.80	205.60
Nb3d3/2 E_b (eV)	209.31	210.88	208.56
r_i (%)	77.28	5.99	16.73

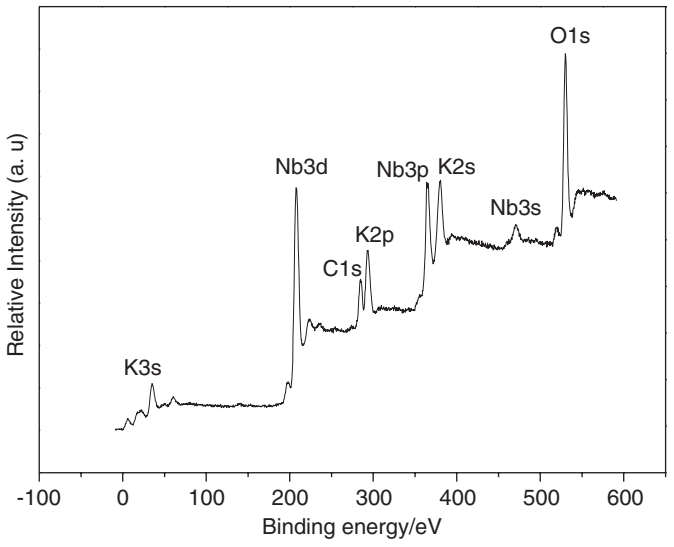

Fig. 5. XPS survey spectrum of the Nb3d region of the catalyst.

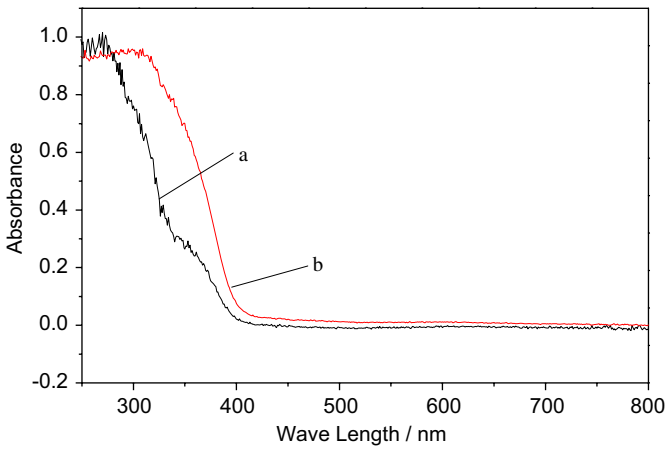

Fig. 6. Diffuse reflectance spectrum of the as-prepared catalyst (a) by the wet chemical method and (b) by the solid-state reaction.

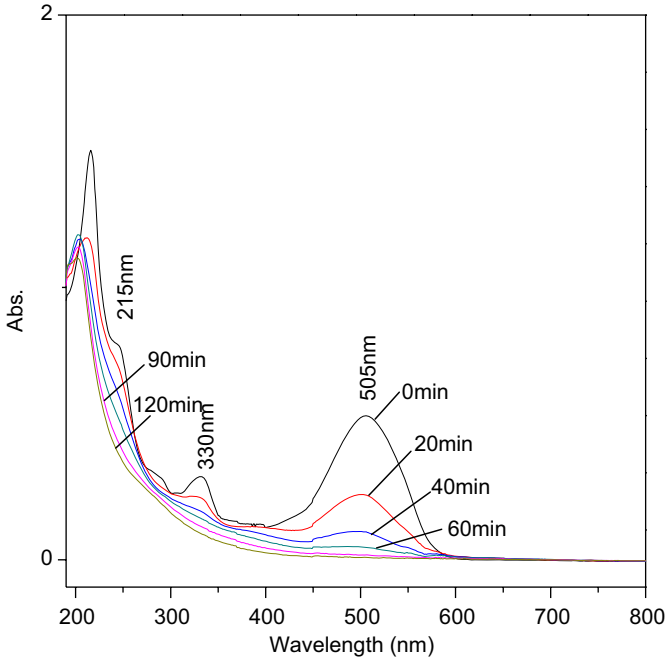

Fig. 7. UV–Vis absorption spectra changes of acid red G solution during the photocatalytic process by $K_6Nb_{10.8}O_{30}$ at different irradiation time.

irradiation. The changes in the absorption spectra of acid red G solution during the photocatalytic process by $K_6Nb_{10.8}O_{30}$ at different irradiation time were measured by UV–Vis spectrometer (UV-2102/PC). As shown in Fig. 7, there are three distinctive peaks at 215, 330 and 505 nm, which correspond to the structure of benzene ring, naphthalene ring and the nitrogen to nitrogen double bond, respectively. The decrease of absorption peaks of acid red G at $\lambda_{max} = 505$ nm in the figure means the nitrogen to nitrogen double bond was destroyed. The peaks of benzene ring and naphthalene ring disappeared gradually with increasing the reaction time, which indicated that photocatalytic degradation also destroyed the benzene and naphthalene rings.

The FT-IR patterns of the catalyst before and after the degradation are shown in Fig. 8, which indicate that no residual acid red G was detected on the recovered sample and the decrease of acid red G in the reaction solution was caused by the photocatalysis but not by the adsorption.

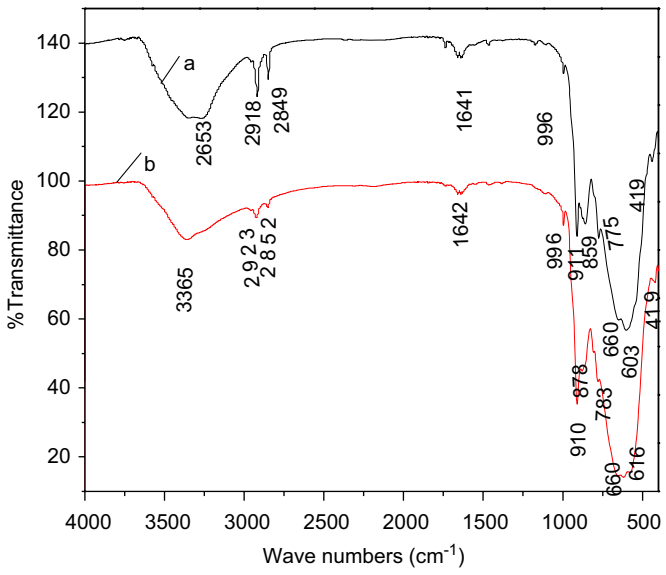

Fig. 8. FT-IR spectra of samples (a) before degradation and (b) after degradation.

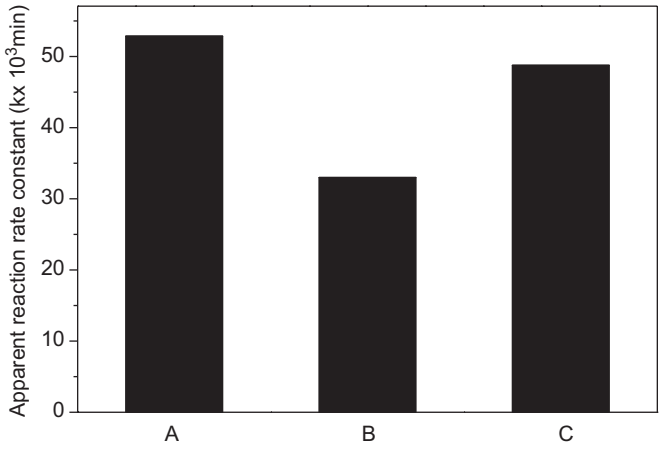

Fig. 9. The reaction rate constants of the catalyst (A) prepared using the wet chemical method; (B) synthesized by the solid-state reaction; (C) P25-TiO_2.

The photocatalytic degradation reactions of acid red G on the catalyst are a pseudo-first-order reaction and its kinetics may be expressed as [37]

$$\ln(C_0/C_t) = k(\mathrm{min}^{-1})t + a \quad \text{(b)}$$

where k is the apparent reaction rate constant, C_0 is the initial concentration of aqueous acid red G, C_t is the concentration of aqueous acid red G at the reaction time of t. Fig. 9 shows the apparent reaction rate constant. The BET surface area of the $K_6Nb_{10.8}O_{30}$ powders prepared by wet chemical method is higher than that of the sample by prepared by the solid-state reaction, which is 3.0 and 2.2, respectively. The results of XRD, SEM, FESEM analyses indicate that the particles obtained by wet chemical method are with much smaller size and uniform shape and show quantum size effect, which may help to create more active sites for photocatalytic reactions and improve the photocatalytic activity of the $K_6Nb_{10.8}O_{30}$ powders. Although the BET surface area of the $K_6Nb_{10.8}O_{30}$ powders obtained by wet chemical method is much lower than that of P25-TiO_2 which has a surface area of about 51 m^2/g, its photocatalytic activity is slightly higher than that of P25-TiO_2. The highly distorted surface NbO_6 octahedral sites always play an important role in heterogeneous catalysis [38]. The different binding energy of niobium in various niobium oxides determines its properties. The behavior of most oxidation catalysts can be explained within the framework of a redox mechanism (reduction–oxidation). The stabilization of niobium and the mobility of active oxygen are important for the catalytic properties of Nb oxides. In the redox catalysis, too high stability of Nb can decrease the reducibility of niobium. A lot of Nb^{4+} cations which exist in $K_6Nb_{10.8}O_{30}$ may be good for increasing the distortion of NbO_6 octahedra in the structure of the compound and improving its photocatalytic property.

4. Conclusion

The TB-type $K_6Nb_{10.8}O_{30}$ powders were successfully prepared by the wet chemical method using niobium oxide and potassium nitrate as raw materials, in which the hydrothermal method was used to dissolve niobium oxide to prepare niobic acid. The as-prepared $K_6Nb_{10.8}O_{30}$ powders are with nanometer size particles and uniform shape and its band gap energy was about 2.92 eV and shows a blue-shift. XPS analysis indicates the different valence states niobium exists in the crystal structure of the photocatalyst, which may be benefit for increasing the photocatalytic activity. The apparent reaction rate constant of the $K_6Nb_{10.8}O_{30}$ catalyst prepared by wet chemical method is much larger than that of the sample synthesized by solid-state reaction and its photocatalytic activities is slightly higher than that of P25-TiO_2. The photocatalytic degradation not only destroyed the nitrogen double bond (–N═N–), but also destroyed the benzene and naphthalene rings. The kinetics of photocatalytic degradation of acid red G follows first-order kinetics equation.

Acknowledgments

This work was supported by the National Natural Science Foundation of China (50472017), National Basic Research Program of China (973 Program) 2007CB613302 and NCET05-0662.

References

[1] N. Daneshvar, H. Ashassi-Sorkhabi, M.B. Kasiri, J. Hazard Mater. 112 (2004) 55.
[2] N. Hilal, G. Busca, F. Rozada, N. Hankins, Desalination 185 (2005) 297.
[3] E. Guibal, J. Roussy, React. Funct. Polym. 67 (2007) 33.
[4] M.R. Ghezzar, F. Abdelmalek, M. Belhadj, N. Benderdouche, A. Addou, Appl. Catal. B: Environ. 72 (2007) 304.
[5] S.F. Chen, Y.Z. Liu, Chemosphere 67 (2007) 1010.
[6] N. Daneshvar, D. Salari, A.R. Khataee, J. Photochem. Photobiol. A 157 (2003) 111.
[7] D.M. Chen, D. Yang, Q. Wang, Z.Y. Jiang, Ind. Eng. Chem. Res. 45 (2006) 4110.
[8] C.H. Wu, K.S. Huang, J.M. Chern, Ind. Eng. Chem. Res. 45 (2006) 2040.
[9] H.K. Singh, M. Saquib, M.M. Haque, M. Muneer, J. Hazard Mater. 142 (2007) 425.
[10] T. Zhong, J.L. Tang, M.K. Zhu, Y.D. Hou, H. Wang, H. Yan, J. Cryst. Growth 285 (2005) 201.
[11] G.K. Zhang, J. Gong, X. Zou, F.S. He, H. Zhang, Q. Zhang, Y. Liu, X. Yang, B. Hu, Chem. Eng. J. 123 (2006) 59.
[12] G.K. Zhang, F.S. He, X. Zou, J. Gong, H.B. Tu, H. Zhang, Q. Zhang, Y. Liu, J. Alloys Compd. 427 (2007) 82.
[13] J.H. Ye, Z.G. Zou, A. Matsushita, Int. J. Hydrogen Energ. 28 (2003) 651.
[14] B. Muktha, J. Darriet, G. Madras, T.N. Guru Row, J. Solid State Chem. 179 (2006) 3919.
[15] H. Takahashi, M. Kakihana, Y. Yamashita, K. Yoshida, S. Ikeda, M. Hara, K. Domen, J. Alloys Compd. 285 (1999) 77.
[16] M. Liu, D. Xue, Solid State Ionics 177 (2006) 275.
[17] M. Liu, D. Xue, C. Luo, J. Am. Ceram. Soc. 89 (2006) 1551.
[18] M.W. Pitcher, Y. He, P.A. Bianconi, Mater. Chem. Phys. 90 (2005) 57.
[19] Z. Cheng, K. Ozawa, A. Miyazaki, H. Kimura, Chem. Lett. 33 (2004) 1620.
[20] M. Liu, D. Xue, K. Li, J. Alloys Compd. 449 (2008) 28.
[21] M.N. Liu, D.F. Xue, C. Luo, J. Alloys Compd. 426 (2006) 118.
[22] Z. Cheng, K. Ozawa, A. Miyazaki, H. Kimura, Chem. Lett. 33 (2004) 1620.
[23] E.R. Camargo, M. Kakihana, Solid State Ionics 151 (2002) 413.

[24] G.K. Zhang, X. Zou, J. Gong, F.S. He, H. Zhang, Q. Zhang, Y. Liu, X. Yang, B. Hu, J. Alloys Compd. 425 (2006) 76.
[25] P. Becker, P. Held, Z. Kristallogr. 215 (2000) 319.
[26] M. Lundberg, M. Sundberg, J. Solid State Chem. 63 (1986) 216.
[27] J.F. Marco, J.R. Gancedo, F.J. Berry, Poyhydron 16 (1997) 2957.
[28] A.L. Cabrera, F. Vargas, J.J. Albers, Surf. Sci. 336 (1995) 280.
[29] J. Kubacki, A. Molak, E. Talik, J. Alloys Compd. 328 (2001) 156.
[30] S.M. M Ramos, B. Canmut, P. Thevenard, D.B. Poker, J. Phys. Chem. Solids 57 (1996) 513.
[31] K. Tabata, T. Choso, Y. Nagasawa, Surf. Sci. 408 (1998) 137.
[32] V.V. Atuchin, I.E. Kalabin, V.G. Kesler, N.V. Pervukhina, J. Electron Spectrosc. Relat. Phenom. 142 (2005) 129.
[33] K. Tabata, M. Kamada, T. Choso, H. Munakata, Appl. Surf. Sci. 125 (1998) 93.
[34] G.K. Zhang, X. Zou, J. Gong, F.S. He, H. Zhang, S.X. Ouyang, H.X. Liu, Q. Zhang, Y. Liu, X. Yang, B. Hu, J. Mol. Catal. A: Chem. 255 (2006) 109.
[35] N. Kumadal, N. Kinamura, Eur. J. Solid State Inorg. Chem. 34 (1997) 65.
[36] A.L. Cabrera, F. Vargas, J.J. Albers, Surf. Sci. 336 (1995) 280.
[37] D.F. Ollis, Environ. Sci. Technol. 19 (1985) 480.
[38] M. Ziolek, Catal. Today 78 (2003) 47.